

Characteristics of heat flow and geothermal fields in Ruidian, Western Yunnan Province, China

Junjie Ba¹, Chuntian Su¹, Yanqing Li¹, Shuiyun Tu^{2*}

¹ Institute of Karst Geology, CAGS/Key Laboratory of Karst Dynamics, MNR&GZAR, Guilin 541004, China

² Yunnan Geological Engineering Exploration Group Co. Ltd., Kunming 650041, China

Corresponding Author Email: tushuiyun7712@163.com

<https://doi.org/10.18280/ijht.360407>

ABSTRACT

Received: 19 January 2018

Accepted: 18 June 2018

Keywords:

ruidian geothermal field, reservoir temperature, heat flow, geothermal gradient

As an important parameter, the temperature of the thermal reservoir is essential to the classification of the geothermal system and the potential of geothermal resources. The inversion coupling study of the geothermal field is an important basis for establishing the genetic model for the geothermal field of Ruidian, Western Yunnan Province, China. With a geothermal flow of up to 120.5mW/m², and an average geothermal gradient of 4.61°C/100m, the Tengchong-Ruidian area is a high temperature geothermal area, where the highest hot spring water temperature can reach 91.5°C. The geothermal reservoirs there can be divided into shallow and deep thermal reservoirs. By using the Log (Q/K) curve method and the Na-K-Mg triangle diagram method, this paper finds that the underground hot water in the study area is in an unsaturated state and mixed with cold water. Then it calculates the thermal reservoir temperature and analyzes the deep temperature characteristics of the subsurface thermal fluid and the mixing process of the hot and cold water using the SiO₂ solubility geothermometer, the dissolved chloride-enthalpy plot, the dissolved silica-enthalpy graph, and the linear regression equations iteration solution methods. The conclusion obtained from this study is that the temperature of the shallow thermal reservoir is about 145°C, that the temperature of the deep thermal reservoir about 220°C, and that the proportion of cold water mixed generally between 60% and 70%. The comprehensive research results of the temperature field in the study area provide theoretical and data support for the establishment of the genetic mechanism for the Ruidian geothermal field.

1. INTRODUCTION

China reserves the second largest amount of geothermal resources in the world, which has a significant prospect for development and utilization. With the traditional energy running short, the need for clean energy is becoming more urgent, leading to more and more attention to the development and utilization of geothermal energy. Currently, the development and utilization of geothermal energy is increasing at a rate of 10% per year in China [1-2]. Due to the great development potential and broad prospects, the sustainable development and utilization has become the most critical issue in the geothermal industry around the world [3-4]. However, the reservoir temperature in the Ruidian geothermal field, as the key parameter in the research and development of underground hot water, is difficult to measure directly [5-6].

The determination of the heat storage temperature is mainly accomplished by two methods: direct measurement method and temperature calculation method. The former delivers more accurate data, but it is also time consuming and costly. Therefore, in most cases, the temperature calculation method is used to obtain the heat storage temperature [7]. Currently, the geothermal thermometric scale /geothermometer approach is an economical and effective way to obtain this parameter. It has been widely used in estimating temperatures, including

cationic, silica, gas chemistry and isotope geothermometers [8-10].

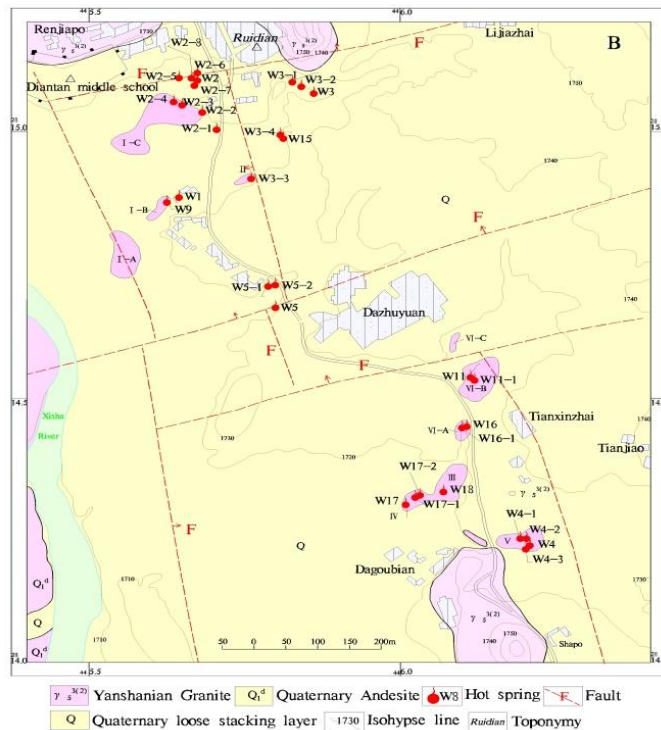
The temperature distribution characteristics of the geothermal field is an important basis for establishing the genetic model for the Ruidian geothermal field. The calculation of the thermal reservoir temperature and the study of the hot fluid mixing mode provide important support for establishing the genetic model for the Ruidian geothermal field.

2. GEOLOGICAL SETTING

The Ruidian geothermal area is a remote area in the western part of Yunnan Province, close to the border with Myanmar (Figure 1A). It is situated on the east end of the Tibet-Yunnan geothermal zone and on the northern margin of the Tengchong volcanic area, which is part of the Tengchong block that developed along the eastern collision boundary between the Indian and Eurasian plates [11]. Being located 50 km north of Tengchong county, the main heat display area of the Ruidian geothermal field is in the Axin Street-Dagoubian zone (Figure 1B). There 39 hot springs have been discovered, many of which are spring clusters. The highest hot spring water temperature can reach 91.5°C, which is the characteristic of the high-energy geothermal resources.



(a)



(b)

Figure 1. (A) Location of the Ruidian geothermal field. (B) Hydrogeological map of the Ruidian geothermal field.

The Ruidian geothermal field is located in the north of the Tengchong synclinorium in the Tengchong fold belt of Gaoligong Mountain. The Tengchong complex is composed of mixed lithologic rocks and granites, and the remaining Upper Paleozoic strata are distributed in intermediate-acidic composite intrusions. The meso-eruptive rocks and craters of the third and quaternary systems cover part of the south and north Tengchong. The study area is a north-south intermountain basin. The Xisha River runs from the north to the south and flows south into the Longchuan River. The stratigraphic distribution, tectonic lines and hydrothermal activities of the Ruidian geothermal field are all controlled by the regional geological structure (Figure 1B). Until the early Cenozoic, this area experienced intense tectonic activities, forming numerous volcanoes and extensive faults [12].

The geothermal flow in the Tengchong-Ruidian area can reach up to 120.5 mW/m^2 , which is about twice the global average (61.6 mW/m^2). Similar to the situation of geothermal heat distribution, the geothermal gradient in the Tengchong area averages $4.61^\circ\text{C}/100 \text{ m}$, which is the highest value in the province [13]. The geothermal gradient of the borehole temperature measurement in the Ruidian geothermal field in the study area is relatively high, generally reaching $30^\circ\text{C}/100 \text{ m}$, with more significant geothermal anomaly.

Based on the systematic study of the geological structure characteristics, the Ruidian geothermal field can be divided into high-temperature thermal reservoirs in the deep granite weathering zone and thermal reservoirs in the lower pale gravel and pebble layers.

3. TEMPERATURE CALCULATION OF SHALLOW GEOTHERMAL RESERVOIR

The temperature of the geothermal reservoir is a key parameter to analyze the formation causes of geothermal systems and to evaluate the potential of the geothermal resources. In the literatures, numerical studies have been conducted to formulate, calibrate and improve the geochemical thermometric scale, including Eillis and Mahon's studies in 1964, 1966 and 1970; Trsdell and Fournier's in 1966, 1970, 1973, 1976 and 1977 and Arnorsson's in 1970, 1985 and 2000. More than a dozen of geothermometer models have been developed to study the temperature of the geothermal reservoir, e.g., SiO_2 , cationic, inert gas and isotope geothermometers [14-18].

The sampling was completed in 2016. During sampling, the water temperatures and pH values were measured on-site by portable measuring instruments; the water sample used for SiO_2 determination was diluted 5 times immediately after being collected, and then stored in a 100 mL polyethylene bottle; the water samples used for other tests were put into 100 mL polyethylene bottles after the suspended substances were removed. The water samples must fill up the sampling bottles to prevent gas from entering. The hydrochemical characteristics of the hot spring samples in Ruidian are shown in Table 1.

Table 1. Chemical characteristics of water samples from hot springs in the Ruidian geothermal area

Hot spring No.	pH	T ($^\circ\text{C}$)	Ca^{2+} mg/L	K^+ mg/L	Mg^{2+} mg/L	Ca^{2+} mg/L	Cl^- mg/L	SO_4^{2-} mg/L	HCO_3^- mg/L	SiO_2 mg/L
W1	7.3	91.5	400.0	37.0	3.6	26.8	153.1	18.0	948.4	134.0
W2	7.1	85.0	375.0	35.5	4.0	32.5	144.6	16.0	929.0	116.0
W3	6.8	75.0	325.0	31.5	3.1	23.8	128.9	15.0	790.8	108.0

W4	6.9	74.0	340.0	30.0	3.8	28.6	138.9	16.0	799.7	130.0
W5	6.5	57.0	230.0	23.0	2.7	15.2	91.6	14.0	535.1	96.0
W9	7.2	72.0	375.0	37.5	3.9	24.9	151.2	24.0	911.5	130.0
W15	8.2	91.0	385.0	38.5	3.7	24.5	155.2	16.0	942.0	150.0
B-ZY1	7.4	87.0	387.0	40.0	3.5	24.6	158.6	17.0	935.0	145.0
B-LX	7.0	75.6	345.0	33.8	3.5	21.8	132.7	24.0	780.3	
B-JZ	7.0	77.0	378.0	35.4	3.8	25.7	159.3	22.0	819.7	
W16	7.2	53.0	290.5	44.0	8.4	6.3	147.6	30.0	559.6	120.0
W16-1	7.7	60.8	355.0	31.5	1.4	12.6	133.6	30.0	778.0	140.0
W17	7.3	58.5	350.0	31.5	2.1	16.1	144.9	20.0	766.6	125.0
ZK14	7.2	67.3	390.0	41.0	4.1	30.0	152.1	30.0	972.5	130.0
T-W1	7.5	86.5	400.0	42.0	3.6	23.6	157.0	16.0	912.0	148.0
T-W2	7.5	87.0	410.0	45.0	4.2	4.5	140.0	31.2	895.0	129.0
T-W3	7.2	77.0	350.0	34.0	3.3	22.2	139.0	32.0	775.0	123.0
T-W4	7.5	81.0	400.0	36.0	3.7	23.6	164.0	24.0	837.0	140.0
T-W5	6.0	56.0	245.0	28.5	3.3	7.5	76.9	14.6	520.0	104.0
T-W17	8.1	64.0	378.0	36.6	2.5	7.5	133.0	25.0	768.0	126.0
Z-JM	8.2	79.3	154.0	39.2	6.5	4.9	181.0	31.8	927.0	160.0
Z-GX	8.5	74.9	165.0	42.9	6.3	4.9	200.0	34.5	939.0	180.0
G-XL	7.6	90.0	326.0	30.8	2.0	15.5	130.9	27.3	928.0	251.8
G-JY	7.0	86.0	290.1	29.2	2.0	20.4	117.6	25.2	906.2	222.6
G-XR	7.5	75.0	250.2	26.6	1.7	17.7	105.0	25.5	752.7	197.1
G-ZY	6.9	85.0	320.2	33.9	2.1	21.6	119.1	27.1	902.2	254.0
L-LX	6.6	73.2	193.5	27.5	2.7	24.7	132.2	13.0	869.5	
L-XX	7.8	68.7	272.8	34.6	2.3	12.5	108.7	13.8	880.3	
L-SP	6.9	62.0	278.5	35.6	2.6	17.6	125.5	19.0	904.6	
L-ZY	6.9	61.6	391.9	83.9	4.1	25.8	165.8	28.2	1016.0	
L-GX	7.4	72.2	388.0	76.0	3.6	17.6	166.4	28.4	1012.9	
L-JZ	6.6	80.0	372.1	75.1	3.6	28.0	156.1	26.8	991.6	
L-JM	7.2	58.3	383.1	75.4	3.6	27.5	161.6	27.8	1006.8	
B-GX	7.5	73.5	421.0	44.0	3.8	21.0	164.0	28.0	983.0	139.0
B-ZY	6.8	82.1	390.0	43.0	4.0	25.0	154.0	27.0	938.0	128.0

3.1 Cationic geothermometer model

The cationic geothermometer model is based on the relationship between the water temperature and the cation ratio per gram in the water, e.g., Ca^{2+} , Mg^{2+} , K^+ , Na^+ , Li^+ . Scholars have developed corresponding cationic geothermometer models to study different geothermal systems [19-21]. The water-rock interactions and mixed convection between waters should be taken into account in the analysis and evaluation on the results of the cationic geothermometer.

3.2 SiO_2 solubility geothermometer model

The SiO_2 solubility geothermometer model is based on the water temperature and the solubility of SiO_2 in the water. It has been widely applied [22]. Arnorsson (1975, 1985 and 2000)

pointed out the relationship between the temperature of the geothermal water and the SiO_2 solubility. The latter is controlled by quartz, chalcedony and both of them when $T > 180^\circ\text{C}$, $T < 110^\circ\text{C}$ and $110^\circ\text{C} < T < 180^\circ\text{C}$, respectively.

3.3 Geothermometer model application condition: Water-rock interaction equilibrium

3.3.1 Log (Q/K)-T curve analysis

The mineral saturation index (Log (Q/K)) is used to estimate the solubility equilibrium of minerals in the water, where Q is the active product and K is the theoretical equilibrium constant. This paper uses the software Phreeqi to produce the log (Q/K)-T curves of anhydrite, aragonite, calcite, chalcedony, chrysotile, domolite, gypsum, quartz and sepiolite in the samples of hot spring W3, as shown in Table 2 and Figure 2.

Table 2. Mineral saturation indices of the water samples from the hot spring in the study area

Number	Anhydrite	Ara gonite	Calcite	Chalce dony	Chry sotile	Domo lite	Gypsum	Halite	Quartz	Sepio lite	Talc
W1	-2.48	0.81	0.92	-0.07	-0.21	1.27	-2.85	-5.98	0.19	-2.51	4.02
W2	-2.53	0.62	0.73	-0.07	-2.02	0.92	-2.81	-6.02	0.20	-3.56	2.15
W3	-2.78	0.11	0.22	-0.02	-4.63	0.00	-2.95	-6.10	0.27	-4.94	-0.44
W4	-1.86	1.23	1.34	0.07	-3.98	1.20	-2.02	-6.08	0.17	-4.33	0.38
W5	-3.13	-0.79	-0.67	0.09	-8.72	-1.56	-3.12	-6.34	0.23	-6.95	-4.47
W9	-2.65	0.51	0.62	0.08	-2.11	0.92	-2.79	-5.97	0.19	-3.00	2.27
W15	-2.77	1.42	1.53	-0.06	5.16	2.70	-3.13	-6.00	0.10	1.09	9.40
W16	-3.28	-0.50	-0.38	0.22	-3.10	-0.10	-3.24	-6.04	0.27	-2.86	1.38
W16-1	-2.96	0.45	0.57	0.21	-1.81	0.71	-2.99	-6.02	0.24	-2.26	2.72
W17	-3.03	0.19	0.32	0.19	-3.66	0.28	-3.03	-5.98	0.22	-3.46	0.80

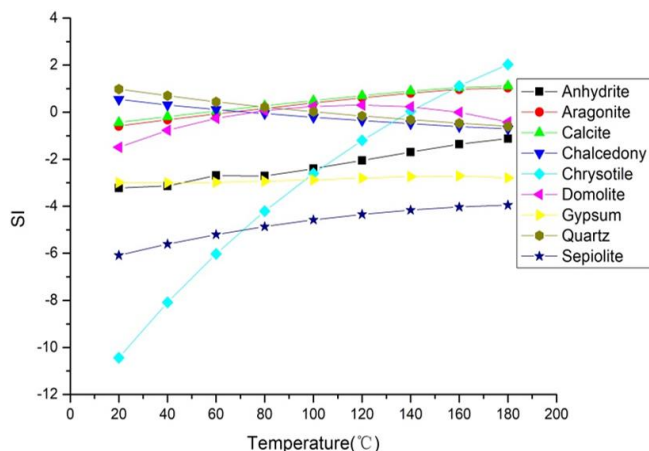


Figure 2. Log (Q/K)-T curves of the mineral solubility equilibrium in hot spring W3

From Figure 2, it is found that the minerals cannot be saturated simultaneously at a certain temperature. This indicates that the hot spring water may mix with cold water when rising and being exposed. Therefore, it is difficult to estimate the precise equilibrium temperature of the hot spring and the mineral solubility equilibrium.

3.3.2 Na-K-Mg triangle diagram analysis

First, the author used Giggenbach's Na-K-Mg triangle diagram to investigate the source of the water, and evaluate the equilibrium of water-rock interactions. Based on this, the author could analyze whether the cationic geothermometer model could be used to calculate the temperature of geothermal fields [23].

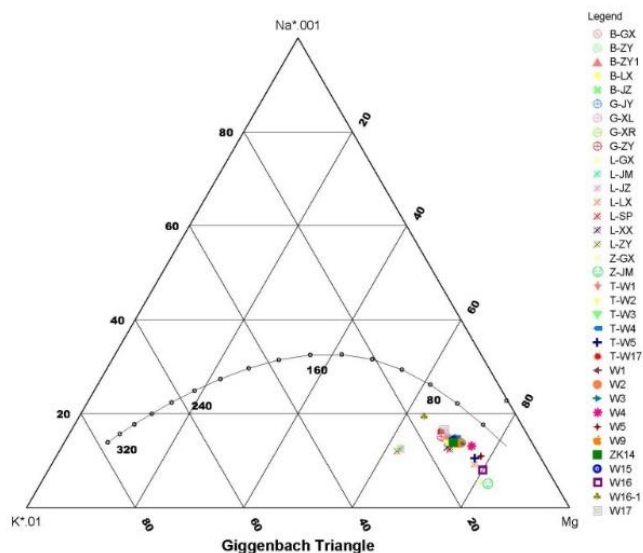


Figure 3. Na-K-Mg triangle diagram of the Ruidian hot springs

Second, this paper used the software Aquachem to produce the Na-K-Mg triangle diagram of the Ruidian hot springs, as shown in Figure 3. It is found that all the hot springs in Ruidian are not mineral-saturated. The estimation results of the

cationic geothermometer model will be negatively biased due to the disequilibrium of mineral solubility and the mix with cold water. Therefore, the cationic geothermometer model is not suitable in this case, and the temperature estimated by this model can only be used as reference.

3.3.3 SiO₂ Solubility Curve Analysis

The concentration of SiO₂ ($\rho(\text{SiO}_2)$, with a unit of mg L⁻¹) in samples are between the curves of chalcedony and amorphous silicon dioxide, as shown in Figure 4. It can be found that the amorphous silicon dioxide shows dissolution disequilibrium while chalcedony and quartz may control the SiO₂ dissolution equilibrium. Therefore, chalcedony and quartz geothermometers are more suitable in estimating the temperature of shallow geothermal reservoirs.

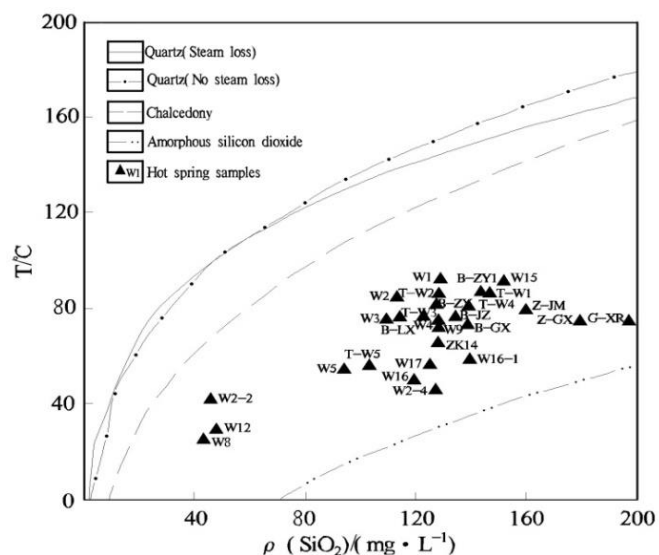


Figure 4. T- $\rho(\text{SiO}_2)$ curves of the hot springs in Ruidian area

3.4 Geothermometer calculation of ruidian geothermal fields

After studying the cationic geothermometer model and the SiO₂ solubility geothermometer model, the author used the Na-K geothermometer and the K-Mg geothermometer at a temperature of 206-221°C and of 105-124°C, respectively. Due to the dissolution disequilibrium of ions, the results from the Na-K geothermometer were higher than the actual values. Then it was used to calculate the temperature of the deep reservoir. However, the limitation of the Mg concentration resulted in lower results than actual values when the K-Mg geothermometer was applied. Therefore, it is not suitable to use the K-Mg geothermometer to calculate the temperature of a high-temperature geothermal field.

According to the above analysis and mineral saturation indices, it is believed that the quartz geothermometer is a conservative method to estimate the temperature of a shallow reservoir. The results from the quartz geothermometer were around 145°C, which can be used as reference data for the shallow reservoir of the Ruidian hot springs. The calculated temperatures by different geothermometers are listed in Table 3.

Table 3. Calculated temperatures from different geothermometer models (°C)

Number	T (Hot spring)	T-K-Mg (Giggenbach, 1986)	T-Na-K-Ca (Fournier and Truesdell, 1973)	T-Na-K (Fournier, 1983)	T-SiO ₂ (Arnorsson, 1985)	T-SiO ₂ (Arnorsson, 2000)
W1	91.5	114.6	168.0	210.3	154.2	154.5
W2	85.0	112.0	158.4	212.3	145.6	145.8
W3	75.0	112.3	160.3	214.3	141.5	141.7
W4	74.0	107.8	152.7	206.4	152.3	152.6
W5	57.0	105.1	154.0	216.9	134.9	135.1
W9	72.0	113.8	170.1	216.9	152.3	152.6
ZK14	67.3	115.9	169.0	221.3	152.3	152.6
W15	91.0	115.5	172.5	216.9	161.1	161.5
W16-1	60.8	124.5	184.2	206.9	156.8	157.2
W17	58.5	117.8	174.9	208.1	150.0	150.3

4. TEMPERATURE CALCULATION OF THE DEEP GEOTHERMAL RESERVOIR

4.1 Sign of hot spring water mixed with cold water

For a high temperature hot spring, Cl⁻ is a reference ion, which can be used to indicate the mixing process of hot spring water and cold water, and also to identify the impacts of other processes on other ions. In the mixing process of the hot spring water with cold water in Ruidian, the concentration of Cl⁻ is in good linear relationships with the concentrations of other ions. Such linear relationships can be analyzed together with the water-rock interactions to find out the impacts of cold water in the mixing process.

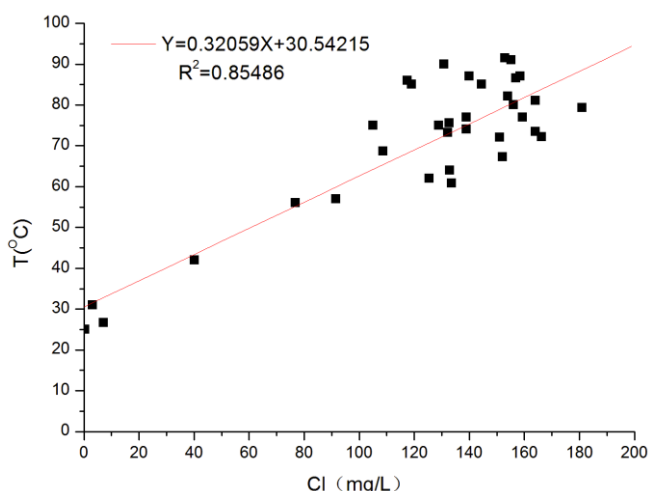


Figure 5. Temperature-Cl⁻ concentration curve of the exposed hot springs in Ruidian area

The concentration of Cl⁻ is positively correlated with the temperature of the hot spring, with a correlation coefficient (R²) of 0.85486, as shown in Figure 5. This correlation also reflects that the hot spring water is mixed with cold water in the rising process.

4.2 Temperature calculation of the geothermal reservoir

4.2.1. Dissolved silica- enthalpy plot

The dissolved silica-enthalpy plot was first proposed by R.O. Fournier and A.H. Truesdell [24]. In this paper, the author chose some sampling spots and prepared the dissolved silica-enthalpy plot to determine the mix proportion of cold water and the possible hot spring temperature. The process of

preparing the dissolved silica-enthalpy plot of the Ruidian geothermal field is shown as follows:

- (1) Ambient temperature: T₀=15°C. The cold water at this temperature did not mix with the hot spring water. The SiO₂ concentration was 16.2 ppm (which is the average concentration of SiO₂ in the water with the temperature ranging between 14-16°C). This was marked as point A in Figure 6.
- (2) Different hot spring temperatures and the corresponding SiO₂ concentrations were marked as point B in Figure 6.
- (3) The AB extension line and the quartz solubility curve cross at point C. From this point, the enthalpy of water in the deep geothermal reservoir can be obtained.
- (4) The line length ratio of BC/AC can be used to calculate the cold water proportion. The concentrations of SiO₂ dissolved in the hot spring water and the water temperatures (listed in Table 1) constitute the dissolved silica-enthalpy plot (Figure 6). According to this figure, the cold water proportion and the enthalpy of the hot fluid can be obtained. The calculated temperatures of the thermal reservoir are shown in Table 4.

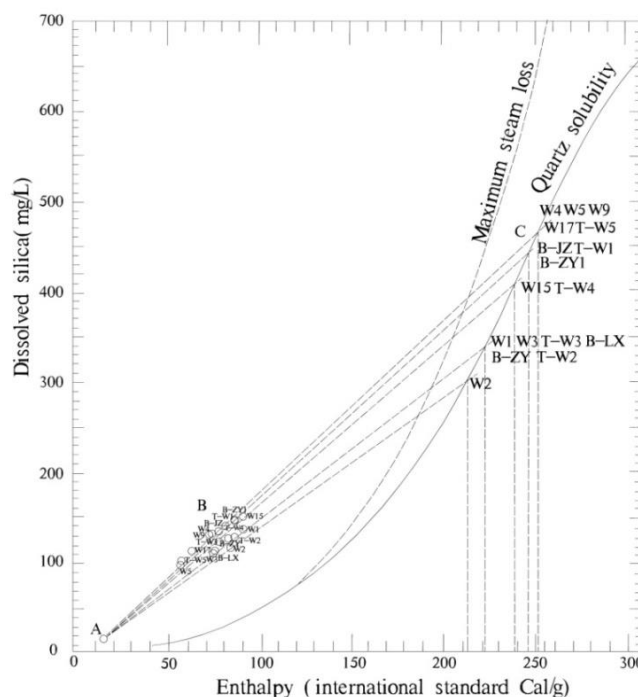


Figure 6. Dissolved silica-enthalpy plot of the Ruidian hot spring (based on Fournier and Truesdell's)

Table 4. Results of the dissolved silica-enthalpy plot of the Ruidian hot spring

Hot spring number	Cold water proportion (%)	The Enthalpy of the deep hot fluid (Cal/g)	Thermal reservoir temperature (°C)
W1	63	226	220
W2	65	214	210
W3	71	223	218
W4	75	257	248
W5	82	257	248

4.2.2 Dissolved chloride-enthalpy plot

The dissolved chloride-enthalpy plot was first proposed by Fournier in 1979. It can not only describe the cooling processes during rising of the hot fluid, but also calculate the temperature of the geothermal fluid (i.e., the initial geothermal fluid in the Ruidian high-temperature geothermal field), which cannot be calculated by any other chemical geothermometer [25].

First, the ambient temperature $T_0=15^\circ\text{C}$. This was the temperature, at which the cold water did not mix with the hot spring water. The Cl^- concentration was 2.09 mg/L in this cold water (which is the average concentration of Cl^- in the water at a temperature ranging between 14-16°C). The author drew the mixed line in the dissolved chloride-enthalpy plot (Figure 7). The mixed line crossed with the steam loss line at a point. The x-coordinate and y-coordinate were the Cl^- concentration and the enthalpy of the initial geothermal fluid, 883J/g. According to the saturated water enthalpy-temperature datasheet, the temperature of the initial geothermal fluid was approximately 217°C.

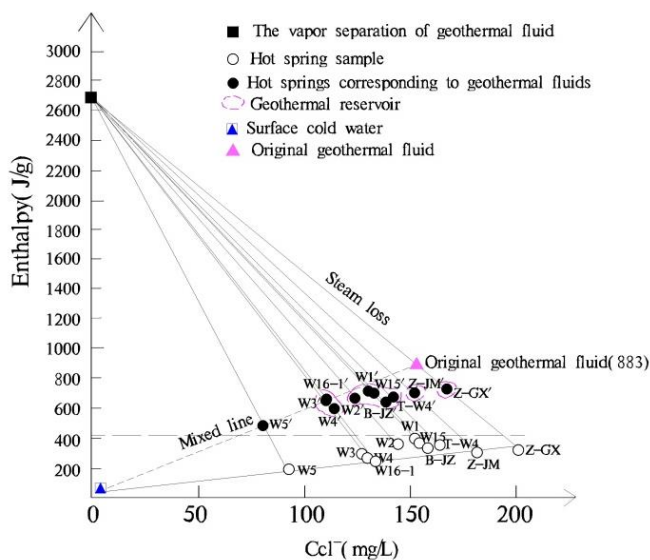


Figure 7. Dissolved chloride-enthalpy plot of Ruidian hot springs (according to nicholson, fournier)

4.2.3 Geothermometer scale plot to calculate the cold water proportion

Considering the mixing with cold water, the SiO_2 (Quartz or Chalcedony) solubility geothermometer model can be applied to calculate the thermal reservoir temperature after the mixing process. In the literatures, some scholars argued that the mixing process had little impact on the Na/K ratio, and that the Na/K geothermometer model can also be used in such

cases [18-20].

The author applied an integrated plot to calculate the temperature of the hot fluid and the mix proportion of the cold water. Take the spot W2 in Ruidian area for example. The temperature of the exposed water was 85°C, and the concentrations of Na^+ and K^+ were 375 and 35 mg/L, respectively. Based on the data, the author calculated the Na/K geothermometer scale to be 211.1°C, and SiO_2 solubility geothermometer scale to be 145.7°C. The ambient temperature was 15°C, and the average concentrations of Na^+ , K^+ and SiO_2 were 3.58, 2.56 and 16.2 mg/L, respectively. Suppose the cold water at 15°C was mixed with the hot fluid, the Na^+ and K^+ concentrations in the hot fluid before the mixing process can be calculated by following equations:

$$\text{Na}_h = \frac{\text{Na}_m - \text{Na}_c X}{1 - X} \quad (1)$$

$$\text{K}_h = \frac{\text{K}_m - \text{K}_c X}{1 - X} \quad (2)$$

where Na_h , Na_m and Na_c are the Na^+ concentrations in the hot fluid, the mixed water and the cold water, respectively. K_h , K_m and K_c are the K^+ concentrations in the hot fluid, the mixed water and the cold water, respectively. X is the cold water proportion. Equations (1)/(2) gives the Na/K ratio before the mixing. This ratio can be used to calculate the standard Na/K geothermometer scale, shown as the line AB in Figure 8. The SiO_2 concentration in the hot fluid before the mixing can also be calculated in the same way.

Line CD and line AB cross at point O. From this point, it was calculated that the mixture of cold water was approximately 64%. Line MN showed the temperature drop during the mixing process, in which temperatures of M and N were 208 and 15°C, respectively. Line MN crosses with line OE at point P. The Y-coordinate of P is the temperature of the hot spring W2 - 86°C, which is very close to the real temperature of the spot W2.

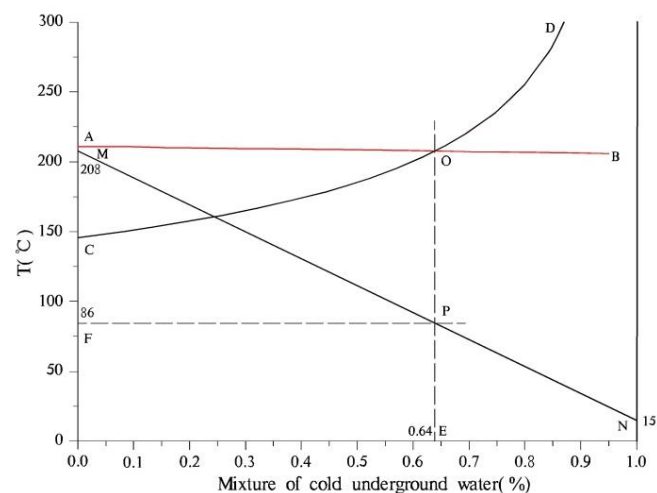


Figure 8. Geothermometer scale plot to calculate the cold water proportion in W2 (according to Tongwei)

4.2.4 Linear regression equations iteration solution

From the above models and calculations, the temperatures of the initial hot fluids, the concentrations of mineral ions and the proportions of cold water in different hot springs can be

estimated. The hot springs in Ruidian are the mixture of the initial hot fluid and the underground cold water and then exposed to the ground. Thus, the author sampled from various hot spring spots and conducted the regression statistical analysis. The linear recursive analysis was performed on the

temperature (T) with concentrations of K^+ , Na^+ , Ca^{2+} , Mg^{2+} , Cl^- , SiO_2 , HCO_3^- , HBO_2^- , F^- and TDS in Origin 9.0. Part of the linear recursive curves are shown in Figures 9-14 and the calculation results listed in Table 5.

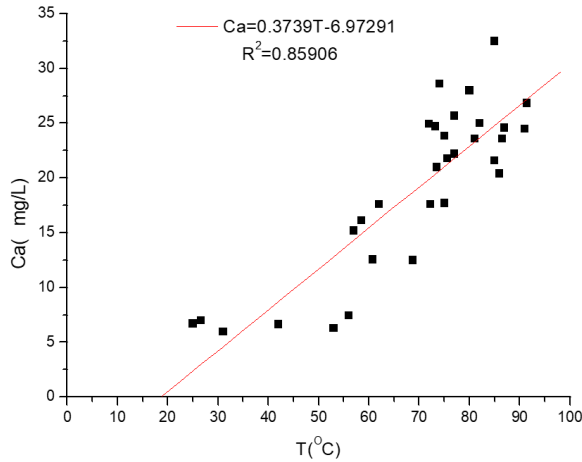


Figure 9. Ca-T linear recursive curve

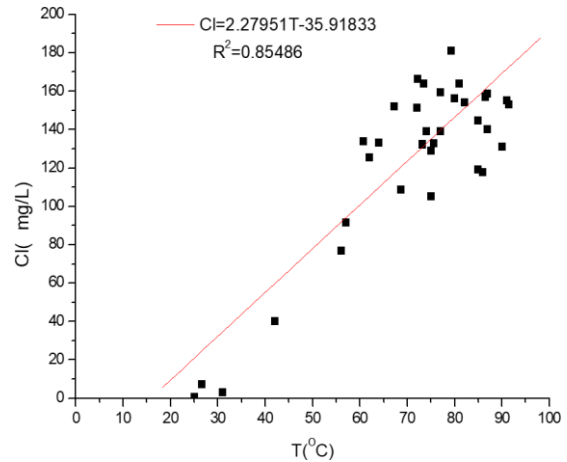


Figure 10. Cl-T linear recursive curve

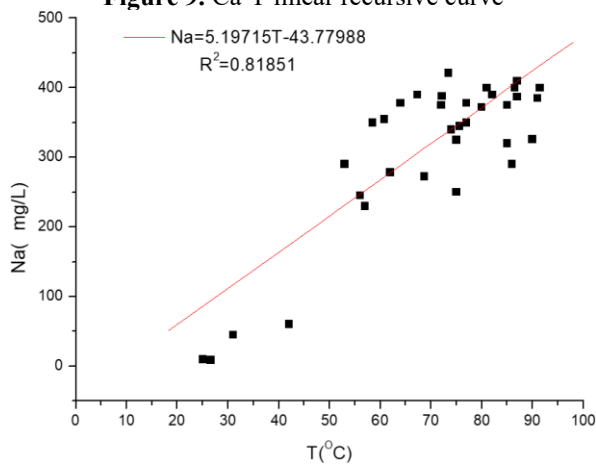


Figure 11. Na-T linear recursive curve

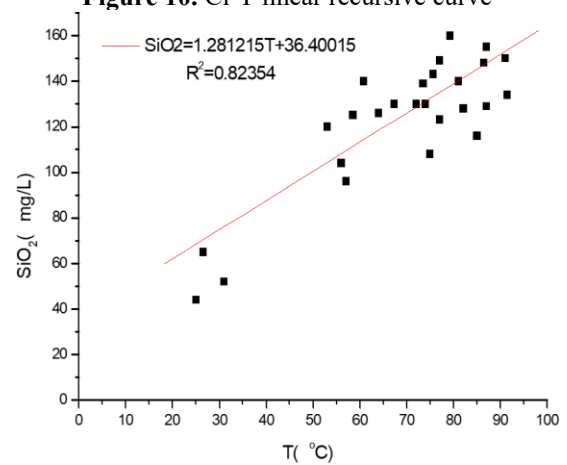


Figure 12. SiO₂-T linear recursive curve

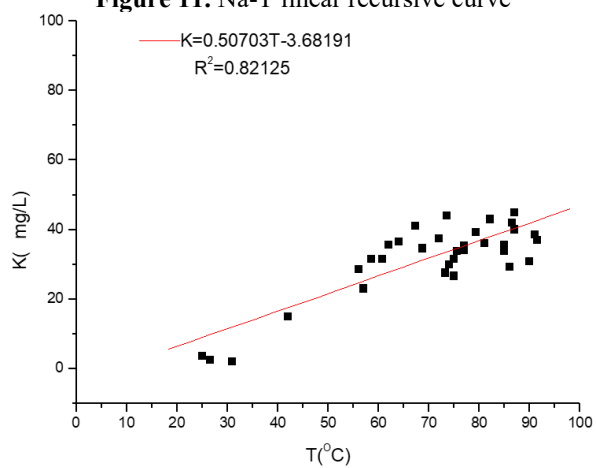


Figure 13. K-T linear recursive curve

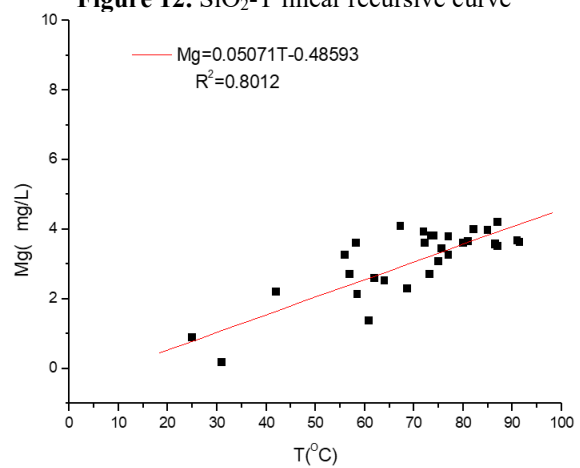


Figure 14. Mg-T linear recursive curve

Table 5. Ion-temperature linear relationship statistics in Ruidian hot springs

Ions	Coefficient	Regression equation	Equation number
Cl-T	0.85486	Cl = 2.27951T - 35.91833	(3)
Na-T	0.81851	Na = 5.19715T - 43.77988	(4)
Mg-T	0.80120	Mg = 0.05071T - 0.48593	(5)
K-T	0.82125	K = 0.50703T - 3.68191	(6)
Ca-T	0.85906	Ca = 0.3739T - 6.97291	(7)
HCO ₃ -T	0.87803	HCO ₃ = 13.70012T - 184.5894	(8)
SiO ₂ -T	0.82354	SiO ₂ = 1.281215T + 36.40015	(9)

According to Fournier’s research in 1981, when SiO₂ achieves dissolution equilibrium, the solubility of SiO₂ in water has the following relationship with temperature T:

$$T=1309/(5.19-\log\text{SiO}_2) - 273.15 \tag{10}$$

Equation (10) is applicable to the conditions with no mixing of underground cold water. If the cold water proportion is 0, Equation (9) becomes (10). Based on Equations (9) and (10), the author calculated the temperature of the initial hot fluid and the concentration of SiO₂:

$$T=211^\circ\text{C}; \text{SiO}_2=306 \text{ mg/L} \tag{11}$$

This temperature (211°C) is very close to the calculated value from the dissolved chloride-enthalpy plot (217°C) and the dissolved silica-enthalpy plot (220°C) (Eq.11). Therefore,

the linear regression equations iteration solution is also accurate and practicable. Substitute T = 211°C into Equations (2)-(10), and the concentrations of other six ions are Na⁺=1052.82, K⁺=103.30, Ca²⁺=71.92, Mg²⁺=10.21, Cl⁻=445.06 and HCO₃⁻=2706.14 mg/L, respectively.

The above values are the ion concentrations in hot springs. Based on the ion concentrations in cold water before mixing with the hot fluid (average concentration in the range of 14-16°C), the cold water proportion in the mixed water are calculated in Table 6. According to this table, the cold water proportions in the exposed Ruidian hot springs are between 66% and 70%, which are close to the values calculated in the Section 4.2. This demonstrates the practicability of the linear regression equations iteration solution. Through the study in this paper, it is estimated that the reasonable temperature of the deep geothermal reservoir is 220°C.

Table 6. Cold water proportions in the mixed water in Ruidian area

Ions	Concentration (mg/L)		Cold water proportion in the mixed water (%)											
	Hot spring	Cold water	W1	W2	W3	W4	W5	W9	W15	W16-1	W17	B-ZY1	B-LX	B-JZ
K ⁺	103.3	2.56	0.66	0.67	0.71	0.73	0.80	0.65	0.64	0.71	0.71	0.63	0.69	0.67
Na ⁺	1052.8	3.58	0.62	0.65	0.69	0.68	0.78	0.65	0.64	0.67	0.67	0.63	0.67	0.64
Ca ²⁺	71.9	9.13	0.72	0.63	0.77	0.69	0.90	0.75	0.76	0.95	0.89	0.75	0.80	0.74
Mg ²⁺	10.2	1.59	0.76	0.72	0.83	0.74	0.87	0.73	0.76	0.68	0.94	0.78	0.78	0.75
Cl ⁻	445.1	2.10	0.66	0.68	0.71	0.69	0.80	0.66	0.65	0.70	0.68	0.65	0.71	0.65
SiO ₂	306.0	16.20	0.59	0.66	0.68	0.61	0.72	0.61	0.54	0.57	0.62	0.52	0.56	0.54
HCO ₃ ⁻	2706.1	7.35	0.65	0.66	0.71	0.71	0.80	0.66	0.65	0.71	0.72	0.66	0.71	0.70
Average			0.67	0.67	0.73	0.70	0.81	0.67	0.66	0.71	0.73	0.66	0.70	0.67

5. CONCLUSIONS

1. The Na-K-Mg triangle diagram and the SiO₂ solubility curves indicate that the cation reaction in the hot water system is not balanced. It is affected by the mixing of cold water. Estimation of the hot spring water temperature in the study area by the cation temperature scale method will result in a lower temperature value, hence the estimation results obtained by the cationic geothermometer model method can only be used as references.

2. By analyzing the use conditions of different temperature scale methods, based on the results of the fluid mineral saturation index, this paper finds it feasible to use the quartz temperature scale as a more conservative method to estimate the temperature of the thermal reservoir in the study area. The calculation results obtained by the quartz temperature scale method are mainly concentrated at about 145°C, which can be used as a reference range for the temperature distribution of the shallow thermal reservoir in the geothermal field in the study area.

3. By using the dissolved silica-enthalpy plot method, silicon enthalpy equation method, dissolved chloride-enthalpy plot method and linear regression equations iteration solution, etc., this paper calculates the temperature of the deep thermal reservoir of the Ruidian geothermal field, which is around 220°C, and also the mix proportion of the cold water, which is generally between 60% and 70%.

ACKNOWLEDGMENT

This work was supported by the National Natural Science Foundation of China (No. 41502342) and the Geological survey project of China (No. DD20160303).

REFERENCES

[1] Guo QH. (2012). Hydrogeochemistry of high-temperature geothermal systems in China: A review.

- Applied Geochemistry 27(10): 1887-1898. <http://dx.doi.org/10.1016/j.apgeochem.2012.07.006>
- [2] Wang GL, Zhang FW, Liu ZM. (2000). An analysis of present situation and prospects of geothermal energy development and utilization in the world. *Acta Geoscientia Sinica* 2(2): 134-139. <http://dx.doi.org/10.3321/j.issn:1006-3021.2000.02.004>
- [3] Ba JJ, Su CT, Li YQ. (2018). A case study on heat source mechanism of high-temperature geothermal field. *Annales de Chimie - Science des Matériaux* 42(1): 129-147. <http://dx.doi.org/10.3166/ACSM.42.129-147>
- [4] Moraci F, Fazia C, Errigo MF. (2018). Smart tools for energy resilient city. *Annales de Chimie - Science des Matériaux* 42(4): 459-470. <http://dx.doi.org/10.3166/ACSM.42.459-470>
- [5] Mongillo MA. (2010). Preface to geothermics special issue on sustainable geothermal utilization. *Geothermics* 39(4): 279-282. <http://dx.doi.org/10.1016/j.geothermics.2010.09.011>
- [6] Fedele R, Merenda M, Praticò FG, Carotenuto F, Corte FGD. (2018). Energy harvesting for IoT road monitoring systems. *Instrumentation, Measure, Métrologie* 17(4): 605-623. <http://dx.doi.org/10.3166/I2M.17.605-623>
- [7] Barbier E. (1997). Nature and technology of geothermal energy: A review. *Renewable & Sustainable Energy Reviews* 1(1): 1-69. [http://dx.doi.org/10.1016/S1364-0321\(97\)00001-4](http://dx.doi.org/10.1016/S1364-0321(97)00001-4)
- [8] Pirlo MC. (2004). Hydrogeochemistry and geothermometry of thermal groundwaters from the Bidsville Track Ridge, Great Artesian Basin, South Australia. *Geothermics* 33(6): 743-774. <http://dx.doi.org/10.1016/j.geothermics.2004.07.001>
- [9] Sun H, Zhang X, Zhou L, Shao X. (2018). Hydration heat and shrinkage of the support of high-performance concrete-filled steel tubes. *Chemical Engineering Transactions* 66: 1171-1176. <http://dx.doi.org/10.3303/CET1866196>
- [10] Govind RR, Vishwambhar SP, Prasad JSVRK. (2018). MHD flow of Powell-Eyring nanofluid containing nanoparticles and gyrotactic microorganisms over a stretched surface. *Revue des Composites et des Matériaux Avancés* 28(3): 405-420. <http://dx.doi.org/10.3166/RCMA.28.405-420>
- [11] Chandrajith R, Barth JAC, Subasinghe ND. (2013). Geochemical and isotope characterization of geothermal spring waters in Sri Lanka: Evidence for steeper than expected geothermal gradients. *Journal of Hydrology* 476(7): 360-369. <http://dx.doi.org/10.1016/j.jhydrol.2012.11.04>
- [12] Kearey P, Wei H. (1993). Geothermal fields of China. *J. Volcanol. Geoth. Res.* 56: 415-428. [http://dx.doi.org/10.1016/0377-0273\(93\)90006-D](http://dx.doi.org/10.1016/0377-0273(93)90006-D)
- [13] Du J, Liu C, Fu B, Ninomia Y, Zhang Y, Wang C, Wang H, Sun Z. (2005). Variations of geothermometry and chemical-isotope compositions of hot spring fluids in the Rehai geothermal field, southwestern China. *J. Volcanol. Geoth. Res.* 142: 243-261. <http://dx.doi.org/10.1016/j.jvolgeores.2004.11.009>
- [14] Zhu M, Tong W. (1987). Surface hydrothermal minerals and their distribution in the Tengchong geothermal area, China. *Geothermics* 16: 181-195. [http://dx.doi.org/10.1016/0375-6505\(87\)90065-4](http://dx.doi.org/10.1016/0375-6505(87)90065-4)
- [15] Fournier R.O. (1977). Chemical geothermometers and mixing models for geothermal systems. *Geothermics* (5): 41-50. [http://dx.doi.org/10.1016/0375-6505\(77\)90007-4](http://dx.doi.org/10.1016/0375-6505(77)90007-4)
- [16] Giggenbach W.F. (1988). Geothermal solute equilibria. Derivation of Na-K-Mg-Ca bioindicators. *Geochimica et Cosmochimica Acta* 52(12): 2749-2765. [http://dx.doi.org/10.1016/0016-7037\(88\)90143-3](http://dx.doi.org/10.1016/0016-7037(88)90143-3)
- [17] Giggenbach W.F. (1980). Geothermal gas equilibria. *Geochimica et Cosmochimica Acta* 44(12): 2021-2032. [http://dx.doi.org/10.1016/0016-7037\(80\)90200-8](http://dx.doi.org/10.1016/0016-7037(80)90200-8)
- [18] Verma SP, Santoyo E. (1997). New improved equations for Na/K, Na/Li and SiO₂ geothermometers by outlier detection and rejection. *Journal of Volcanology and Geothermal Research* 79(1-2): 9-23. [http://dx.doi.org/10.1016/S0377-0273\(97\)00024-3](http://dx.doi.org/10.1016/S0377-0273(97)00024-3)
- [19] Giggenbach WF. (2001). Evaluation of results from the fourth and fifth IAVCEI field workshop on volcanic gases, Vulcano island, Italy and Java, Indonesia. *Journal of Volcanology & Geothermal Research* 108(1): 157-172. [http://dx.doi.org/10.1016/S0377-0273\(00\)00283-3](http://dx.doi.org/10.1016/S0377-0273(00)00283-3)
- [20] Giggenbach W, Sheppard DS, Robinson BW. (1994). Geochemical structure and position of the Waitotapu geothermal field, New Zealand. *Geothermics* 23(5): 599-644. [http://dx.doi.org/10.1016/0375-6505\(94\)90022-1](http://dx.doi.org/10.1016/0375-6505(94)90022-1)
- [21] Giggenbach WF, Sano Y, Wakita H. (1993). Isotopic composition of helium, and CO₂ and CH₄ contents in gases produced along the New Zealand part of a convergent plate boundary. *Geochimica Et Cosmochimica Acta* 57(14): 3427-3455. [http://dx.doi.org/10.1016/0016-7037\(93\)90549-C](http://dx.doi.org/10.1016/0016-7037(93)90549-C)
- [22] Kharaka MSLYK. (1982). Chemical Geothermometers Applied to Formation Waters, Gulf of Mexico and California Basins: ABSTRACT. *Aapg Bulletin* 66: 588. <http://dx.doi.org/10.1306/03B59EAE-16D1-11D7-8645000102C1865D>
- [23] Giggenbach WF. (1988). Geothermal solute equilibria. Derivation of Na-K-Mg-Ca geoindicators. *Geochimica Et Cosmochimica Acta* 52(12): 2749-2765. [http://dx.doi.org/10.1016/0016-7037\(88\)90143-3](http://dx.doi.org/10.1016/0016-7037(88)90143-3)
- [24] Fournier RO, Truesdell AH. (1970). Chemical indicators of subsurface temperature applied to hot spring waters of Yellowstone National Park, Wyoming, U.S.A. *Geothermics* 2: 529-535. [http://dx.doi.org/10.1016/0375-6505\(70\)90051-9](http://dx.doi.org/10.1016/0375-6505(70)90051-9)
- [25] Fournier RO. (1979). Geochemical and hydrologic considerations and the use of enthalpy-chloride diagrams in the prediction of underground conditions in hot-spring systems. *Journal of Volcanology & Geothermal Research* 5(1-2): 1-16. [http://dx.doi.org/10.1016/0377-0273\(79\)90029-5](http://dx.doi.org/10.1016/0377-0273(79)90029-5)